Analysis of the electrical characteristics of Mo/4H-SiC Schottky barrier diodes for temperature sensing applications

K. Zeghdar[1], L. Dehimi[1,2] F. Pezzimenti[3,4], M. L. Megherbi[1], and F. G. Della Corte[3]

1.-Laboratory of Metallic and Semi-conducting Materials (LMSM), University of Biskra, BP 145, 07000 Biskra, Algeria. 2.-Faculty of Material Science, University of Batna, 05000 Batna, Algeria. 3.-DIIES –Mediterranea University, Feo di Vito, Reggio Calabria I-89122, Italy. 4.-e-mail: fortunato.pezzimenti@unirc.it.

The experimental forward current-voltage-temperature (I_D-V_D-T) characteristics of Mo/4H-SiC Schottky barrier diodes (SBDs) are investigated by means of a careful simulation study. The simulations are in excellent agreement with measurements in the whole explored current range extending over ten orders of magnitude for temperatures from 303 K to 498 K. The diode ideality factor tends to decrease while the Schottky barrier height increases with increasing temperature. These variations are explained on the basis of the thermionic emission (TE) theory with a Gaussian distribution of the barrier height (BH) around the Mo/4H-SiC interface. The calculated Richardson constant is A^* = 155.78 Acm^{-2}K^{-2} which is very close to the theoretical value of 146 Acm^{-2}K^{-2} expected for *n*-type 4H-SiC. The linear dependence of V_D on temperature is also investigated for several bias currents. The obtained results reveal that the device is well suited for temperature sensing applications, showing a good coefficient of determination (R^2 = 0.99974 for 100 nA ≤ I_D ≤ 1 mA) and a high sensitivity (S = 1.92 mV/K for I_D = 1 μA). The temperature error between the voltage measurements and their linear best-fit is lower than 1.5 K.

Keywords: 4H-SiC, Schottky barrier diode, ideality factor, temperature, thermionic emission.

INTRODUCTION

Silicon carbide (SiC) is a wide band-gap semiconductor with attractive physical properties for the realization of electronic devices useful for high-temperature, high-power, and high-frequency applications. In particular, the capability of SiC to operate at high-temperature ensures significant lifetime and reliability improvements of devices in many engineering fields such as spacecraft, automotive, and energy production industries [1-7].

Temperature sensors play a key role in many industrial processes and different applications. The most commonly used types of temperature sensors are thermocouples, thermistors, resistance temperature detectors

(RTDs), and semiconductor devices. In more detail, thermocouples are known for their wide temperature range and low drift; thermistors are fast and have high sensitivity; RTDs have good linearity and the highest accuracy and stability. All these devices, however, require a certain amount of interface circuitry and could result difficult to use. On the contrary, diode-based temperature sensors are characterized by low manufacturing costs, full IC compatibility, and almost linear voltage-temperature behaviors that, under specific bias conditions, preserve their sensitivity and accuracy over a wide range of temperature [8]. In fact, in a solid-state junction-based structure several physical parameters are strongly dependent on temperature such as the carrier mobility, the intrinsic carrier concentration, the carrier average energy, and the barrier height.

In this context, Schottky barrier diodes (SBDs) have gained an increasing interest for sensing applications in harsh environments thanks to a high-resolution and chemical inertness [9-13]. The most common metals used for Schottky contacts on SiC are titanium (Ti) and Nickel (Ni), which typically show good reproducibility of the barrier height [14]. However, the large scale diffusion of these structures is limited by some technological issues mainly related to the high density of defects at the semiconductor interface and the high temperatures of the annealing processes [15]. Molybdenum (Mo) can be considered a promising alternative metal. Mo-based SBDs, in fact, show a better behavior in forward bias with a low voltage drop and an ideality factor close to the unity if they are compared with the Ti-based counterparts [16].

Starting from the experimental results on Mo/4H–SiC SBDs reported in [17], in this paper a careful simulation study is performed in order to evaluate the suitability of these devices as temperature sensors. More in detail, the diode forward I_D-V_D curves are fitted in a wide range of temperature extending from 303 K to 498 K by involving different current transport mechanisms. At high current regimes, the diode series resistance is on the order of 16 Ω.

The temperature dependence of the main device electrical parameters, namely the Schottky barrier height (SBH) and ideality factor, is explained with the assumption of a Gaussian distribution of the barrier height around the Mo/4H–SiC interface. In particular, the SBH increases while the diode ideality factor tends to decrease with increasing temperature. Finally, the device performance as temperature sensor is investigated analyzing the grade of linearity of the V_D-T characteristics as well as the diode sensitivity and the temperature root mean square error for different bias currents.

DEVICE STRUCTURE AND SIMULATION SETUP

A schematic cross section of the Mo/4H-SiC Schottky diode considered in this work is shown in Fig. 1. The drawing is not to scale.

The experimental devices are based on a commercial available <0001> n-type 4H–SiC homoepitaxial wafer of elevated crystal quality [18]. The epilayer is 10 μm thick with a donor doping concentration of 1.3×10^{16} cm^{-3}. The Schottky contacts are circular with a diameter of 150 μm. Exhaustive details about the diode fabrication process are provided in [17]. In short, the Schottky contacts are formed by depositing molybdenum (Mo) through an electron-beam (e-beam) lithography evaporation technique at a pressure of 1×10^{-5} Pa. Then, the annealing treatment is performed in an open furnace at 500 °C under a N_2 flow of about 1000 sccm. Finally, the backside ohmic contact of the wafer is formed by e-beam deposition of a 250-nm-thick Mo film.

The numerical simulation analysis of the diode in Fig. 1 was carried out by using the Atals-Silvaco physical simulator [19] to solve the carrier continuity equations and Poisson's equation onto a finely meshed device structure in the cylindrical coordinate system. The fundamental 4H-SiC physical models taken into account include the band-gap temperature dependence and the apparent band-gap narrowing (BGN), the incomplete ionization of dopants, the Shockley–Read–Hall (SRH) and Auger recombination processes, the carrier lifetime and the carrier mobility as a function of temperature and doping, and the Schottky thermionic emission model which involves the field-dependent barrier lowering effect. These models are briefly recalled as follows.

The temperature dependence of the 4H-SiC band-gap is in the form of [20]:

$$E_g(T) = E_{g0} - \alpha(T - 300) \tag{1}$$

where E_{g0} = 3.26 eV is the material band-gap energy assumed at T = 300 K and α = 3.3×10^{-4} eV/K is a specific constant.

According to [21], the incomplete ionization of impurities is given by

$$N_{A,D}^{-+} = N_{A,D}\left(\frac{-1+\sqrt{1+4g_{V,C}\frac{N_{A,D}}{N_{V,C}^{(T)}}e^{\frac{\Delta E_{A,D}}{kT}}}}{2g_{V,C}\frac{N_{A,D}}{N_{V,C}^{(T)}}e^{\frac{\Delta E_{A,D}}{kT}}}\right) \tag{2}$$

where ΔE_A and ΔE_D are the acceptor and donor energy levels, N_A and N_D are the substitutional p-type and n-type doping concentrations, g_v = 4 and g_c = 2 are the degeneracy factors of the valence and conduction band [22], and N_V and N_C are the hole and electron density of states varying with temperature:

$$N_{C,V}(T) = N_{C,V\,300}\left(\frac{T}{300}\right)^{3/2}. \tag{3}$$

Here, $N_{V\,300}$ = 3.29×10^{19} cm^{-3} and $N_{C\,300}$ = 1.66×10^{19} cm^{-3} are the hole and electron density of states at room temperature, respectively.

The apparent band-gap narrowing effect is a function of the activated doping concentration and it is accounted for according to Lindefelt's model of the band edge displacements in the n-type (ΔE_{gn}) and p-type (ΔE_{gp}) regions [23]:

$$\Delta E_{gn,p} = A_{n,p}\left(\frac{N_{D,A}^{+-}}{10^{18}}\right)^{1/2} + B_{n,p}\left(\frac{N_{D,A}^{+-}}{10^{18}}\right)^{1/3} + C_{n,p}\left(\frac{N_{D,A}^{+-}}{10^{18}}\right)^{1/4} \tag{4}$$

where $A_{n,p}$, $B_{n,p}$, and $C_{n,p}$ are the appropriate 4H-SiC parameters [22] listed in Table I.

The SRH and Auger recombination rates are modeled using the standard expressions [24]:

$$R_{SRH} = \frac{np - n_i^2}{\tau_n\left(p + n_i \exp\left(-\frac{E_{trap}}{kT}\right)\right) + \tau_p\left(n + n_i \exp\left(\frac{E_{trap}}{kT}\right)\right)} \tag{5}$$

$$R_{Auger} = \left(C_n n + C_p p\right)\left(np - n_i^2\right) \tag{6}$$

where $C_p = 2\times10^{-31}$ cm^{6}s^{-1} and $C_n = 5\times10^{-31}$ cm^{6}s^{-1} are the Auger coefficients [25], E_{trap} is the difference between the trap energy level and the intrinsic Fermi level, and τ_n and τ_p are the carrier lifetimes modeled through the semi-empirical formula proposed in [26] considering a temperature dependence described by a power law [21,27]:

$$\tau_{n,p} = \frac{\tau_{0n,p}\left(\frac{T}{300}\right)^{\theta_{n,p}}}{1 + \left(\frac{N}{N_{n,p}^{SRH}}\right)}. \tag{7}$$

Here, N is the total doping concentration for a given device region, $\tau_{0n} = 500$ ns and $\tau_{0p} = 100$ ns are process-dependent parameters, and $N_{n,p}^{SRH} = 5\times10^{16}$ cm^{-3} is a reference constant [28].

In order to model the low-field carrier mobility, we use the Caughey-Thomas analytical formula [29,30]:

$$\mu_{n,p} = \mu_{0n.p}^{min}\left(\frac{T}{300}\right)^{\alpha_{np}} + \frac{\mu_{0n.p}^{max}\left(\frac{T}{300}\right)^{\beta_{n.p}} - \mu_{0n\,p}^{min}\left(\frac{T}{300}\right)^{\alpha_{n.p}}}{1 + \left(\frac{T}{300}\right)^{\gamma_{n.p}}\left(\frac{N}{N_{n.p}^{crit}}\right)^{\delta_{n.p}}} \tag{8}$$

where μ_0^{min}, μ_0^{max}, N^{crit}, α, β, γ, and δ are parameters taken from [21,29] and summarized in Table II.

In addition, the mobility degradation due to the carrier saturated drift velocity ($v_{sat} = 2\times10^7$ cm/s) is expressed by means of

$$\mu_{n,p}(E) = \frac{\mu_{n,p}}{\left[1 + \left(E\frac{\mu_{n,p}}{v_{sat}}\right)^{k_{n,p}}\right]^{1/k_{n,p}}} \tag{9}$$

where E is the electric field in the direction of the current flow, $k_n = 2$ and $k_p = 1$ [20].

Finally, the ideal barrier height ($\emptyset_B$) in the device structure is the conventional difference [31]

$$\emptyset_B = (\theta_M - \chi_s) \tag{10}$$

where the metal work function θ_M is fixed to 4.53 eV [17], and the electron affinity χ_s is used as fitting parameter as in [32].

It must be noted that the simulation setup introduced above was used in other recent manuscripts of ours [33-36] and it is supported by experimental results on 4H-SiC-based Schottky and p-i-n diodes [37-42].

RESULTS AND DISCUSSION

Current-voltage characteristics

In this paper, the I_D-V_D experimental curves in forward bias of Mo/4H-SiC SBDs are fitted with the numerical results for nine different temperatures from 303 K to 498 K as shown in Fig. 2 in semi-log scale.

The simulations are in good agreement with the measurements in the whole explored current range extending over ten orders of magnitude. It is important to note that, since during the simulations it has not been modelled an explicit charge density at the metal-semiconductor interface, the interface trap effects could be considered negligible for the samples under test.

As well known, by assuming the thermionic emission (TE) theory, the SBD I_D-V_D expression in forward bias is in the form of [43,44]

$$I_D = I_0 \left[\exp\left(\frac{q(V_D - I_D R_s)}{nkT}\right) - 1\right] \tag{11}$$

where R_s is the series resistance, n is the ideality factor, q is the electronic charge, k is the Boltzmann constant, T is the absolute temperature, and I_0 is the saturation current defined by:

$$I_0 = AA^*T^2 \exp\left(-\frac{q\emptyset_B}{kT}\right). \tag{12}$$

Here, $\emptyset_B$ is the barrier height, A is the effective area of the diode for current transport, and A^* is the Richardson constant that takes into account the tunneling phenomena with a theoretical value of 146 $Acm^{-2}K^{-2}$ expected for n-type 4H-SiC [45].

The fundamental diode parameters, namely R_s, $\emptyset_B$, and n can be extracted from the I_D–V_D-T curves in Fig. 2 similarly to [46].

More in detail, R_s is calculated in the high-current regime (I_D > 1 mA) and its temperature dependence is shown in Fig. 3.

The R_s value is between 14.75 Ω and 16.8 Ω. This variation can be explained by considering that with an increasing temperature more and more impurities are ionized and the enhanced scattering mechanisms penalize the carrier mobility leading, therefore, to a decreased conductivity of 4H-SiC [47].

Concerning the barrier height, we calculate $\emptyset_B = (kT/q)\ln(AA^*T^2/I_0)$ from (12) once I_0 was determined as the intercept of the plot $\ln(I_D)$ vs. V_D for $V_D = 0$ at each temperature. At the same time, n is extracted determining the slope of the linear region of the curves $\ln(I_D)$ vs. V_D at low bias voltages according to

$$n = \frac{q}{kT}\frac{dV}{d(\ln I)} . \tag{13}$$

The obtained $\emptyset_B$ and *n* behaviors at different temperatures are plotted in Fig. 4.

Although, the barrier height and the ideality factor variation with temperature are rather limited appearing in the order of a few percentage points, $\emptyset_B$ tends to increase while *n* decreases with increasing temperature. In particular, $\emptyset_B$ ranges from about 1.1 eV to 1.17 eV and *n* from 1.071 to 1.047 resulting very close to the ideal value (*n* = 1).

By considering (12) in the form of $\ln(I_0/T^2) = \ln(AA^*) - (q/kT)\emptyset_B$, Fig. 5 shows the Arrhenius plot of the term $\ln(I_0/T^2)$ against 1000/*T*.

As we can see, a perfect linear fit of the $\ln(I_0/T^2)$ data allows to calculate the Richardson constant A^* from the intercept at the ordinate. It results A^* = 3.67 $Acm^{-2}K^{-2}$ which is much lower than the theoretical value of 146 $Acm^{-2}K^{-2}$. Finally, from the slope of the linear fit we obtain an activation energy of 1.013 eV.

These results seem to predict current transport mechanisms not following the pure TE theory. In fact, the temperature dependence of $\emptyset_B$ and *n*, as well as the small value of A^* reported above, can be explained by assuming the existence of a Schottky barrier inhomogeneity at the Mo/4H-SiC interface that consists of low and high barrier areas due to a non-uniformity distribution of the interfacial charges as suggested by Werner and Guttler in [48]. More in detail, this spatial inhomogeneity at the diode contact is described by a Gaussian distribution of the SBH, $\rho(\emptyset_B)$, with a standard deviation, σ, around a mean value, $\overline{\emptyset_B}$, in the form of

$$\rho(\emptyset_B) = \frac{1}{\sigma\sqrt{2\pi}}\exp\left[-\frac{(\emptyset_B - \overline{\emptyset}_B)^2}{2\sigma^2}\right] \tag{14}$$

where the pre-exponential term is a normalization constant, and $\overline{\emptyset}_B$ and σ are linearly bias-dependent parameters as follows:

$$\overline{\emptyset_B} = \overline{\emptyset}_{B0} + \rho_2 V_D \tag{15}$$

$$\sigma^2 = {\sigma_0}^2 + \rho_3 V_D . \tag{16}$$

Here, $\overline{\emptyset}_{B0}$ and σ_0 are the zero-bias reference values, and ρ_2 and ρ_3 are temperature-independent coefficients which model the voltage deformation of the barrier distribution.

The total current across the diode junction at a forward bias voltage V_D is then calculated as:

$$I_D = \int i_D(V_D, \emptyset_B)\rho(\emptyset_B)d\emptyset_B \tag{17}$$

where $i_D(V_D, \emptyset_B)$ is the current component for a given barrier height. By introducing $i_D(V_D, \emptyset_B)$ and $\rho(\emptyset_B)$ from (11) and (14) into (17) and performing the integration we obtain:

$$I_D = I_0\left[\exp\left(\frac{q(V_D - I_D R_s)}{n_{ap}kT}\right) - 1\right] \tag{18}$$

where

$$I_0 = AA^*T^2\exp\left(-\frac{q}{kT}\emptyset_{Bap}\right). \tag{19}$$

Here, $\emptyset_{Bap}$ and n_{ap} are the apparent SBH and the ideality factor in the form of

$$\emptyset_{Bap} = \overline{\emptyset}_{B0} - \frac{q\sigma_0^2}{2kT} \tag{20}$$

$$\frac{1}{n_{ap}} = 1 - \rho_2 + \frac{q\rho_3}{2kT}. \tag{21}$$

Moving from these expressions, the Schottky barrier inhomogeneity can be characterized by plotting both $\emptyset_{Bap}$ and n_{ap} vs. $q/2kT$ as shown in Fig. 6 and Fig. 7, respectively.

In Fig. 6, the linear best-fit of $\emptyset_{Bap}$ gives $\overline{\emptyset}_{B0}$ = 1.262 eV from the intercept at the ordinate and σ_0 = 90.5 mV from the slope. We can note that $\overline{\emptyset}_{B0}$ is slightly greater than the uniform value calculated previously and the standard deviation σ_0, which is a measure of the Schottky barrier inhomogeneity, is not negligible. In fact, a lower σ_0 corresponds to a more homogeneous SBH.

Similarly, from the plot of the term $(n_{ap}^{-1} - 1)$ in Fig. 7 we calculate the coefficient ρ_2 = 0.015 from the intercept and ρ_3 = -2.6 mV from the slope of the straight line which fits the diode datas. These values are consistent with literature on 4H-SiC-based SBDs emphasizing a Gaussian distribution of the barrier height at the Mo/4H–SiC interface [49-51].

Finally, by combining (19) and (20), we can write the following expression

$$ln\left(\frac{I_0}{T^2}\right) - \left(\frac{q^2\sigma_0^2}{2k^2T^2}\right) = \ln(AA^*) - \left(\frac{q\overline{\emptyset}_{B0}}{kT}\right) \tag{22}$$

which is useful to calculate the modified Richardson plot, i.e. $\ln(I_0/T^2) - (q^2\sigma_0^2/2k^2T^2)$ vs. q/kT, as shown in Fig. 8. We calculate $\overline{\emptyset}_{B0}$ = 1.265 eV and A^* = 155.78 Acm^{-2}K^{-2} from the slope and the intercept at the ordinate of the linear best-fit, respectively. It is important to note that $\overline{\emptyset}_{B0}$ is in excellent agreement with the results in Fig. 6.

At the same time, the modified Richardson constant is much closer to the expected theoretical value of 146 $Acm^{-2}K^{-2}$.

Mo/4H-SiC SBD as temperature sensor

The performance of the investigated SBD as a sensor of temperature is evaluated by forward biasing the device at a constant current level in the range from 10 nA up to 1 mA.

The diode voltage behaviors as a function of temperature for six different values of I_D are shown in Fig. 9. Here, the sensor sensitivity (S) calculated at each current level is also reported. As we can see, thanks to an almost constant value of the ideality factor, the diode experimental V_D-T characteristics exhibit a good degree of linearity in the whole explored temperature range.

From (11), we can write

$$V_D = \frac{kT}{q} n \ln\left(\frac{I_D}{I_0}\right) + R_s I_D \ . \tag{23}$$

The sensor sensitivity is defined as the temperature derivative of (23) and it can be obtained from the slope of the straight-lines in Fig. 9 resulting, for example, S = 1.29 mV/K for I_D = 1 mA. This value increases almost monotonically up to S = 2.24 mV/K for I_D = 10 nA.

In more detail, starting from (23) we can state that, for a fixed I_D, the V_D dependence on T is linear if a) the R_s effect is negligible, b) I_0 is negligible compared to I_D, and c) n can be considered constant with T. Referring to Fig. 2, it is evident that biasing the diode at appropriately low currents could help meeting the first requirement, also for a wider operating temperature range of the sensor in both the cold and hot regimes. In addition, although R_s is a temperature-dependent parameter, the resulting value of R_s could be minimized acting on the conductive characteristics of the epilayer and substrate (i.e., doping and thickness) without changing the diode Schottky barrier structure meaningfully. Concerning the second requirement, we have to consider that the saturation current increases by increasing the temperature. In particular, from the simulations of the diodes under test, I_0 tends to become comparable to the supposed driving current for T > 523 K, thus compromising the sensor linearity. Finally, discussing the third requirement, from Fig. 4 we can see that, although the ideality factor is rather constant with T in the investigated temperature range, n tends to diverge at low temperatures and this result discourages, de facto, the use of the sensor for T < 273 K.

In order to assess the agreement between the V_D-T experimental data and the corresponding linear best-fit, the coefficient of determination (R^2), which quantifies the correlation of the measurements to a straight-line [52], and the corresponding temperature error (e_T) are calculated. More in detail, R^2 is assumed in the form of

$$R^2 = 1 - \frac{\sum_{j=1}^{i}(V_{D,j} - f_{l,j})^2}{\sum_{j=1}^{i}(V_{D,j} - \overline{V_D})^2} \quad (24)$$

where $i = 9$ is the number of the different temperatures imposed during the measurements, $\overline{V_D}$ is the resulting mean voltage, and $V_{D,j}$ and $f_{l,j}$ are the j-values provided by the experimental data and their linear best-fit at each j-temperature. The R^2 and S behaviors as a function of the diode forward current are shown in Fig. 10.

It can be noted that R^2 is quite constant around its maximum value of 0.9997 for I_D exceeding 100 nA leading to a temperature sensor with a highly linear behavior in a wide range of biasing currents up to 1 mA, namely until the series resistance effects can be considered negligible even at the highest temperatures. For $I_D < 100$ nA, the leakage phenomena within the device structure increasingly affect the R^2 value as the temperature increases.

The use of the linear approximation model of the V_D-T characteristics leads to a temperature estimation affected by an error calculated according to

$$e_T = S^{-1}\sqrt{i^{-1}\sum_{j=1}^{i}(V_{D,j} - f_{l,j})^2} \quad (25)$$

where, for the different set points considered in this work, e_T is rather independent on the probe current in a wide range of values (i.e., 100nA ≤ I_D ≤ 1mA) resulting always lower than 1.5 K as shown in Fig. 11. In particular, the highest linearity errors are recognized at $T = 448$ K.

The obtained results in terms of e_T are consistent with literature data on 4H-SiC-based Schottky diodes [53,54]. In addition, they are not too far from the calculations relative to high-performance platinum RTDs in the hot regime ($T > 473$ K) [55], which exhibit a linearity error close to 0.38% per Celsius degree.

CONCLUSION

In this paper, we have investigated the I_D-V_D-T characteristics of Mo/4H-SiC SBDs in order to fix the temperature effect on the main device electrical parameters. In particular, the experimental curves have been fitted from 303 K to 498 K by means of a careful simulation analysis achieving an excellent agreement in the whole explored current range. The diode ideality factor appears very close to the unity (1.071 at $T = 303$ K) and it tends to decreases as the temperature increases. On the other hand, the barrier height increases with temperature. These behaviors has been interpreted on the basis of the TE theory with a Gaussian distribution of the barrier height at the metal-semiconductor interface.

By considering the impressive degree of linearity of the experimental data until the diode series resistance effects as well as the leakage phenomena can be considered negligible, the device performance as temperature sensor has been evaluated. For a forward bias current that spans from 100 nA to 1 mA, the simulation results

showed a good coefficient of determination ($R^2 = 0.99974$) and a high sensitivity value of 1.92 mV/K for $I_D = 1$ µA. The temperature error calculated between the voltage measurements and their linear best-fit is in the limit of 1.5 K.

REFERENCES

[1] F. G. Della Corte, G. De Martino, F. Pezzimenti, G. Adinolfi, and G. Graditi, *IEEE Trans. Electron Dev*. 65, 3352 (2018).

[2] A. Leon-Masich, H. Valderrama-Blavi, J. M. Bosque-Moncusi, and L. Martinez-Salamero, *IEEE Trans. Power Electron.* 31, 1633 (2015).

[3] H. Bencherif, L. Dehimi, F. Pezzimenti, and F. G. Della Corte, *Appl. Phys. A-Mater.*125, 294 (2019).

[4] G. De Martino, F. Pezzimenti, and F. G. Della Corte, in Proc. *International Semiconductor Conference – CAS* (2018), pp. 147-150.

[5] J. Fabre, P. Ladoux, and M. Piton, *IEEE Trans. Power Electron.* 30, 4079 (2014).

[6] F. Pezzimenti, S. Bellone, F. G. Della Corte, and R. Nipoti, *Mater. Sci. Forum* 740, 942 (2013).

[7] H. Bencherif, L. Dehimi, F. Pezzimenti, G. De Martino, and F. G. Della Corte, *J. Electron. Mater.* 48, 3871 (2019).

[8] M. Mansoor, I. Haneef, S. Akhtar, A. De Luca, and F. Udrea, *Sens. Actuators A, Phys.* 232, 63 (2015).

[9] S. Rao, G. Pangallo, F. Pezzimenti, and F. G. Della Corte, *IEEE Electron Dev. Lett.* 36, 720 (2015)

[10] F. Bouzid, L. Dehimi, and F. Pezzimenti, *J. Electron. Mater*. 46, 6563 (2017).

[11] G. Pristavu, M Badila, F. Draghici, R. Pascu, F. Craciunoiu, I. Rusu, and A. Pribeanu *Mater. Sci. Forum* 897, 606 (2017).

[12] F. Bouzid, L. Dehimi, F. Pezzimenti, M. Hadjab, and A. H. Larbi, *Superlattice. Microst*. 122, 57 (2018).

[13] N. Zhang, C. Lin, D. Senesky, and A. Pisano, *Appl. Phys. Lett.* 104, 073504 (2014).

[14] K. Zekentes, and K. Vasilevskiy, Advancing silicon carbide electronics technology I: Metal Contacts to Silicon Carbide: Physics, Technology, Applications (Milleserville: Materials Research Forum LLC, 2018).

[15] S. Kyoung, E. S. Jung, and M. Y.Sung, *Microelectron. Eng.* 154, 69 (2016).

[16] D. Perrone, M. Naretto, S. Ferrero, L. Scaltrito, and C. Pirri, *Mater. Sci. Forum* 615, 647 (2009).

[17] L. Boussouar, Z. Ouennoughi, N. Rouag, A. Sellai, R. Weiss, and H. Ryssel, *Microelectron. Eng.* 88, 969 (2011).

[18] CREE Research Inc. Durham, NC, USA http://www.cree.com. Accessed 1 March 2019.

[19] Silvaco Int., *Atlas User's Manual,* Device Simulator Software (2016).

[20] X. Li, Y. Luo, L. Fursin, J. H. Zhao, M. Pan, P. Alexandrov, and M. Wein, *Solid State Electron.* 47, 233 (2003).

[21] M. Ruff, H. Mitlehner, and R. Helbig, *IEEE Trans. Electron Dev.* 41, 1040 (1994).

[22] F. Pezzimenti, L. F. Albanese, S. Bellone, and F. G. Della Corte, in Proc. *IEEE Bipolar/BiCMOS Circuits and Technology Meeting – BCTM* (2009), pp. 214-217.

[23] U. Lindefelt, *J. Appl. Phys.* 84, 2628 (1998).

[24] S. Selberherr, Analysis and Simulation of Semiconductor Devices (Wien: Springer, 1984).

[25] A. Galeckas, J. Linnros, V. Grivickas, U. Lindefelf, and C. Hallin, *Appl. Phys. Lett.* 71, 3269 (1997).

[26] P. T. Landsberg, and G. S. Kousik, *J. Appl. Phys.* 56, 1696 (1984).

[27] F. Pezzimenti, *IEEE Trans. Electron Dev.* 60, 1404 (2013).

[28] M. Bakowski, U. Gustafsson and U. Lindefelt, *Phys. Stat. Sol. (a)* 162, 421 (1997).

[29] M. Roschke, and F. Schwierz, *IEEE Trans. Electron Dev.* 48, 1442 (2001).

[30] F. Pezzimenti, and F. G. Della Corte, in Proc. *Mediterranean Electrotechnical Conf. - MELECON* (2010), pp. 1129-1134.

[31] S M Sze, Physics of semiconductor devices. 2nd ed. (New York: John Wiley and Sons,1982)

[32] M. Philip, and A. O'Neill, in Proc. *IEEE Conf. on Optoelectronic and Microelectronic Materials and Devices* (2006), pp. 137-140.

[33] A. Fritah, L. Dehimi, F. Pezzimenti, A. Saadoune, and B. Abay, *J. Electron Mater.* 48, 3692 (2019).

[34] F. Pezzimenti, H. Bencherif, A. Yousfi and L. Dehimi, *Solid-State Electron.* 161, 107642 (2019).

[35] Y. Marouf, L. Dehimi, F. Bouzid, F. Pezzimenti, and F. G. Della Corte, *Optik* 163, 22 (2018).

[36] M. L. Megherbi, F. Pezzimenti, L. Dehimi, M. A. Saadoune, and F. G. Della Corte, *IEEE Trans. Electron Dev.* 65, 3371 (2018).

[37] K. Zeghdar, L. Dehimi, F. Pezzimenti, S. Rao, and F. Della Corte, *Jpn. J. Appl. Phys*. 58, 014002 (2019).

[38] M. L. Megherbi, F. Pezzimenti, L. Dehimi, A. Saadoune, and F. G. Della Corte, *J. Electron. Mater.* 47, 1414 (2018).

[39] G. De Martino, F. Pezzimenti, F. G. Della Corte, G. Adinolfi, and G. Graditi, in Proc. *IEEE Int. Conf. Ph. D. Research in Microelectronics and Electronics - PRIME* (2017), pp. 221-224.

[40] F. Pezzimenti, and F. G. Della Corte, In Proc. *International Semiconductor Conference – CAS* (2012), pp. 347-350.

[41] F. G. Della Corte, F. Pezzimenti, S. Bellone, and R. Nipoti, *Mater. Sci. Forum*, 679, 621 (2011).

[42] M. L. Megherbi, F. Pezzimenti, L. Dehimi, S. Rao, and F. G. Della Corte, *Solid-State Electron.* 109, 12 (2015).

[43] H. Cetin, and E. Ayyildiz, *Physica B* 405, 559 (2010).

[44] F. Bouzid, F. Pezzimenti, L. Dehimi, M. L. Megherbi, and F. G. Della Corte, *Jpn. J. Appl. Phys*. 56, 094301 (2017).

[45] M. J. Bozack, Phys. Status Solidi B 202, 549 (1997).

[46] S. K. Cheung, and N. W. Cheung, *Appl, Phys, Lett*. 49, 85 (1986).

[47] Q. W. Song, Y. M. Zhang, Y. M. Zhang, F. P. Chen, and X. Y. Tang, *Chinese Phys. B* 20, 057301 (2011).

[48] J. H. Werner, and H. H. Guttler, *J. Appl. Phys.* 69, 1522 (1991).

[49] D. J. Ewing, Q. Wahab, R. R. Ciechonski, M. Syvajarvi, R. Yakimova, and L. M. Porter, *Semicond. Sci. Tech*. 22, 1287 (2007).

[50] J. M. Bluet, D. Ziane, G. Guillot, D. Tournier, P. Brosselard, J. Montserrat, and P. Godignon, Superl. Microst. 40, 399 (2006).

[51] M. E. Aydin, N. Yildirim, and A. Türüt, *J. Appl. Phys*. 102, 043701 (2007).

[52] N. J. D. Nagelkerke, *Biometrika* 78, 691 (1991).

[53] F. Draghici, G. Brezeanu, G. Pristavu, R. Pascu, M. Badila, A. Pribeanu, and E.Ceuca, *Sensors* 19, 2384 (2019).

[54] L. Di Benedetto, G. D. Licciardo, S. Rao, G. Pangallo, F. Della Corte, and A. Rubino, *IEEE Trans. Electron Dev.* 65, 687 (2018)

[55] R. Radetić, M. Pavlov-Kagadejev, and N. Milivojević, *Serb. J. Electr. Eng.* 12, 345 (2015).

This is a post-peer-review, pre-copyedit version of an article published in Journal of Electronic Materials, 2020, 49(2), pp. 1322–1329. The final authenticated version is available online at: http://dx.doi.org/10.1007/s11664-019-07802-6

Figure captions

Fig. 1. Mo/4H-SiC SBD schematic cross section.

Fig. 2. Mo/4H-SiC SBD measured (symbols) and simulated (solid lines) I_D-V_D curves at different temperatures.

Fig. 3. Temperature dependence of the series resistance.

Fig. 4. Ideality factor and barrier height behaviors as a function of temperature.

Fig. 5. Arrhenius plot of $\ln(I_0/T^2)$ vs. 1000/T.

Fig. 6. $\emptyset_{Bap}$ vs. $q/2kT$ according to a Gaussian distribution of the SBH.

Fig. 7. $(n_{ap}^{-1} - 1)$ vs. $q/2kT$ according to a Gaussian distribution of the SBH.

Fig. 8. $\ln(I_0/T^2) - (q^2\sigma_0^2/2k^2T^2)$ vs. q/kT according to a Gaussian distribution of the SBH.

Fig. 9. V_D-T characteristics for different values of I_D.

Fig. 10. Sensor sensitivity and coefficient of determination as a function of the forward current.

Fig. 11. Temperature linearity error.

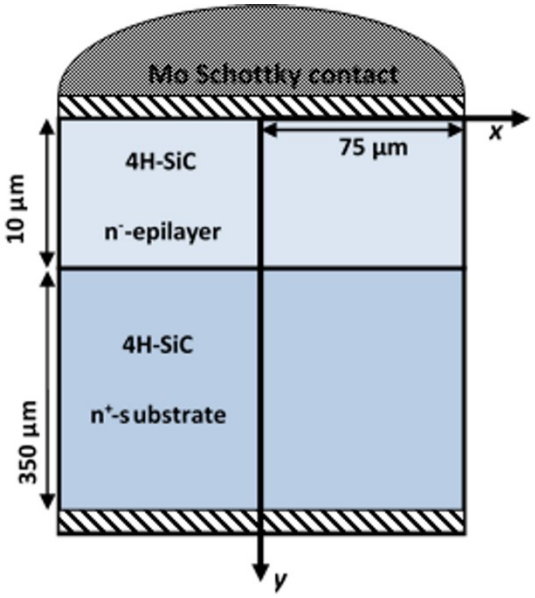
Mo Schottky contact
75 µm
x
4H-SiC
n⁻-epilayer
10 µm
4H-SiC
n⁺-substrate
350 µm
y

Fig. 1

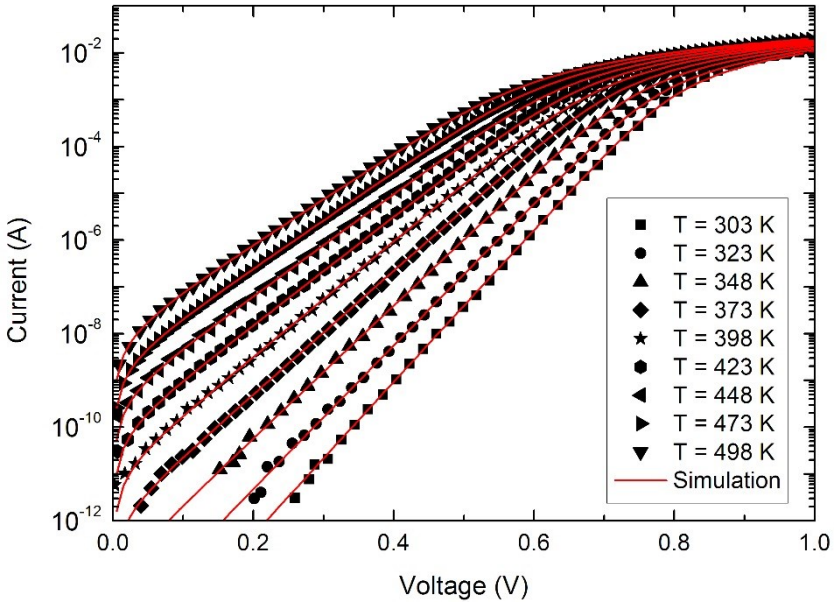
Current (A)
Voltage (V)
T = 303 K
T = 323 K
T = 348 K
T = 373 K
T = 398 K
T = 423 K
T = 448 K
T = 473 K
T = 498 K
Simulation

Fig. 2

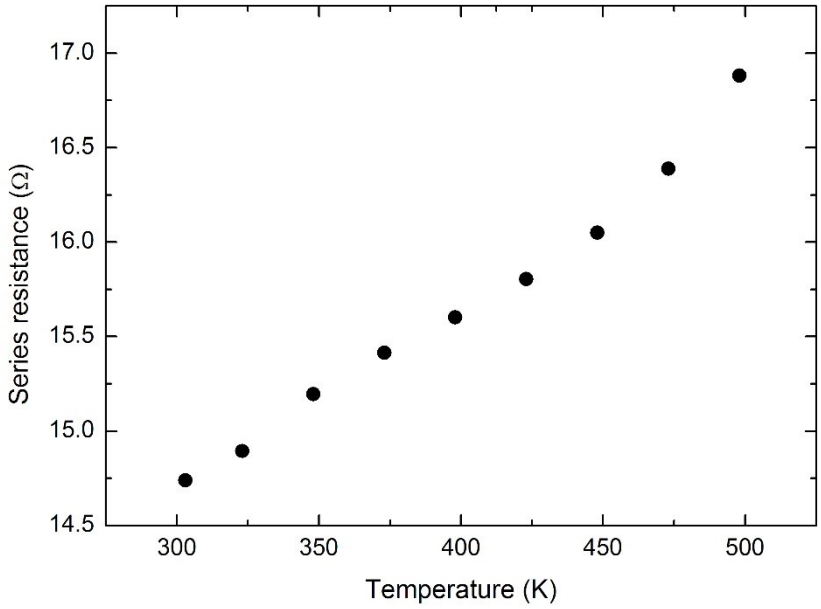
17.0
16.5
16.0
15.5
15.0
14.5
Series resistance (Ω)
300
350
400
450
500
Temperature (K)

Fig. 3

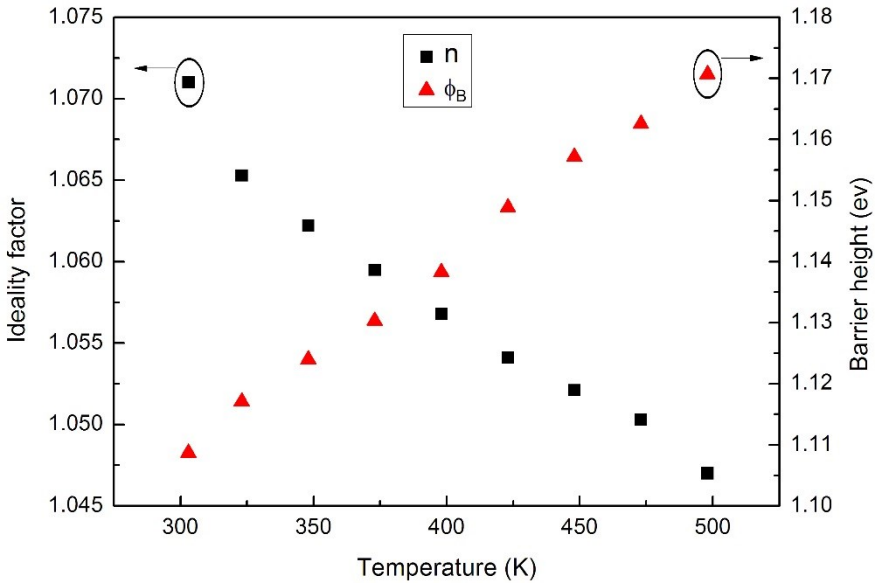
n
ϕ_B
Ideality factor
Barrier height (ev)
Temperature (K)
1.075
1.070
1.065
1.060
1.055
1.050
1.045
1.18
1.17
1.16
1.15
1.14
1.13
1.12
1.11
1.10
300
350
400
450
500

Fig. 4

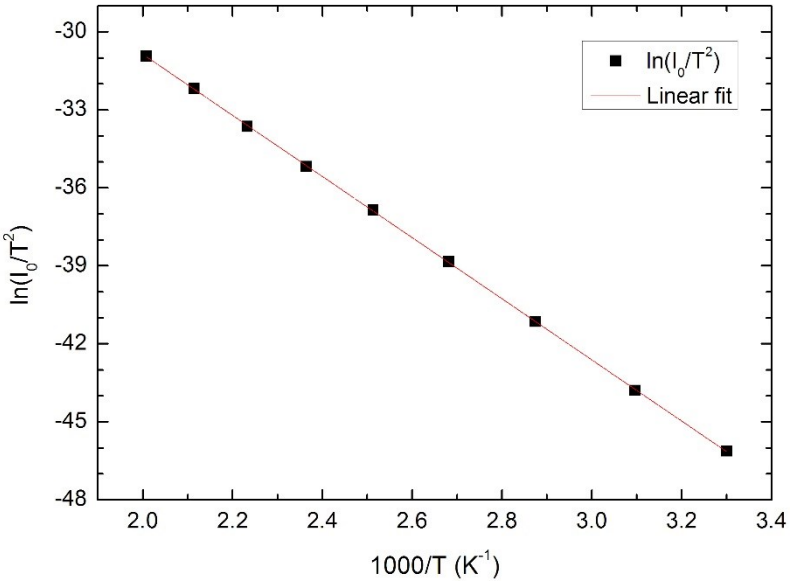
-30
-33
-36
-39
-42
-45
-48
2.0
2.2
2.4
2.6
2.8
3.0
3.2
3.4
ln(I0/T2)
1000/T (K-1)
ln(I0/T2)
Linear fit

Fig. 5

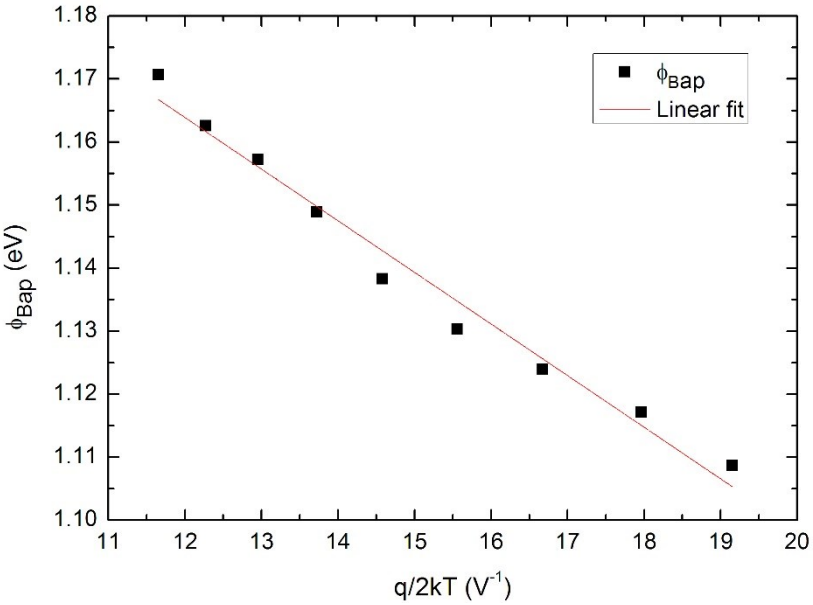
1.18
1.17
1.16
1.15
1.14
1.13
1.12
1.11
1.10
ϕ_{Bap} (eV)
11
12
13
14
15
16
17
18
19
20
q/2kT (V^{-1})
ϕ_{Bap}
Linear fit

Fig. 6

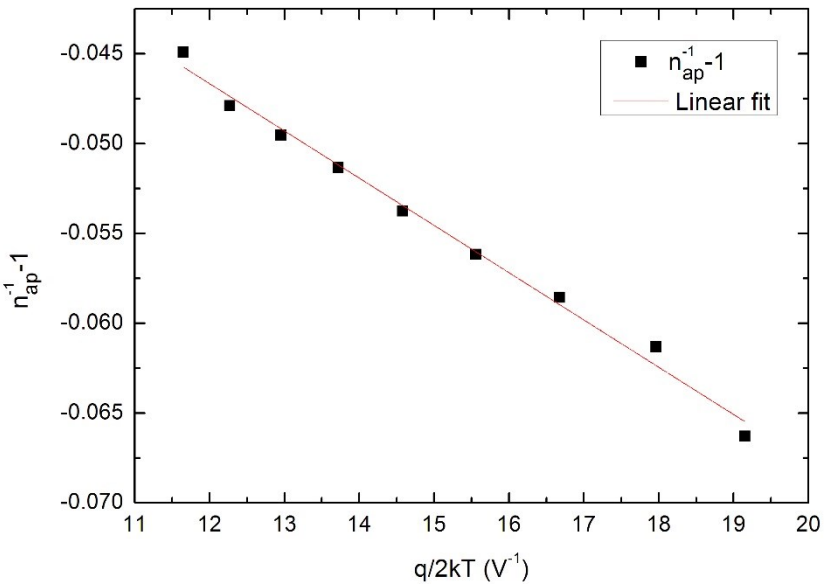
-0.045
-0.050
-0.055
-0.060
-0.065
-0.070
11
12
13
14
15
16
17
18
19
20
n_{ap}^{-1}-1
q/2kT (V^{-1})
n_{ap}^{-1}-1
Linear fit

Fig. 7

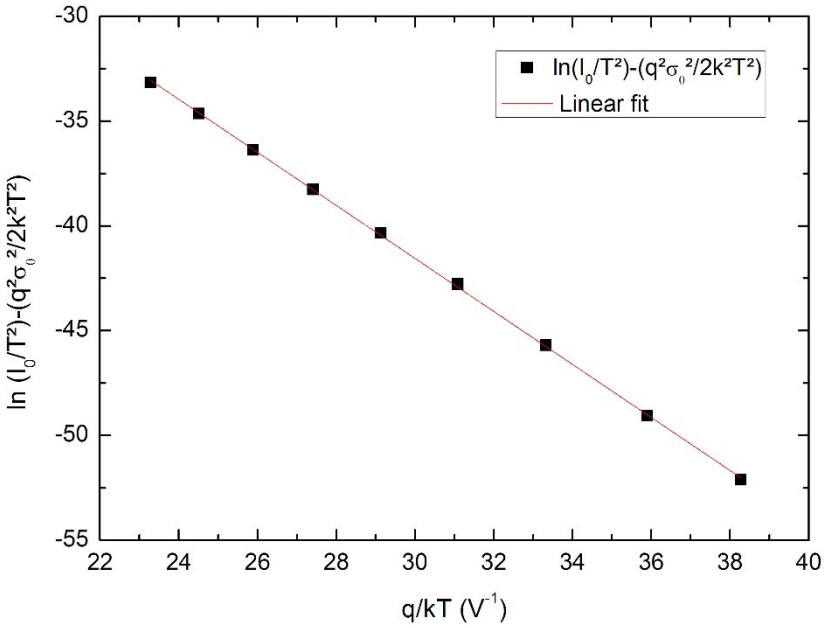
-30
-35
-40
-45
-50
-55
22
24
26
28
30
32
34
36
38
40
ln (I0/T²)-(q²σ0²/2k²T²)
q/kT (V-1)
ln(I0/T²)-(q²σ0²/2k²T²)
Linear fit

Fig. 8

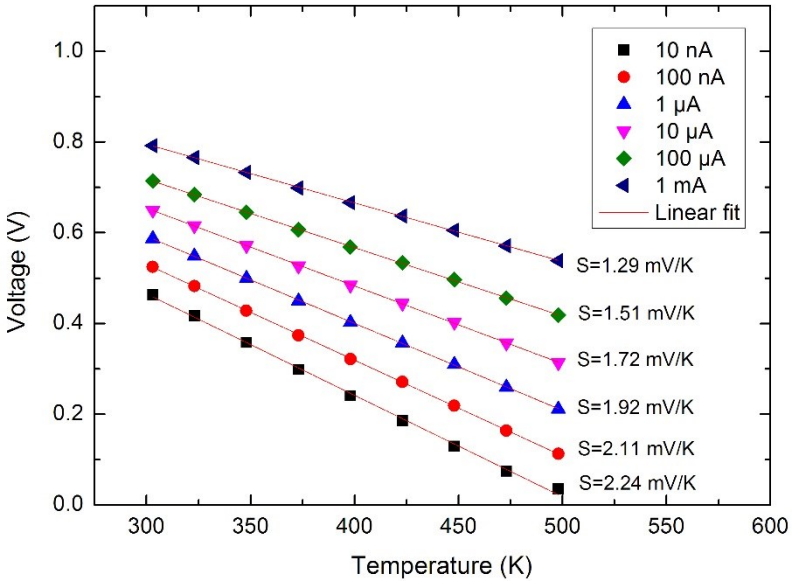
10 nA
100 nA
1 μA
10 μA
100 μA
1 mA
Linear fit
S=1.29 mV/K
S=1.51 mV/K
S=1.72 mV/K
S=1.92 mV/K
S=2.11 mV/K
S=2.24 mV/K
Voltage (V)
Temperature (K)
0.0
0.2
0.4
0.6
0.8
1.0
300
350
400
450
500
550
600

Fig. 9

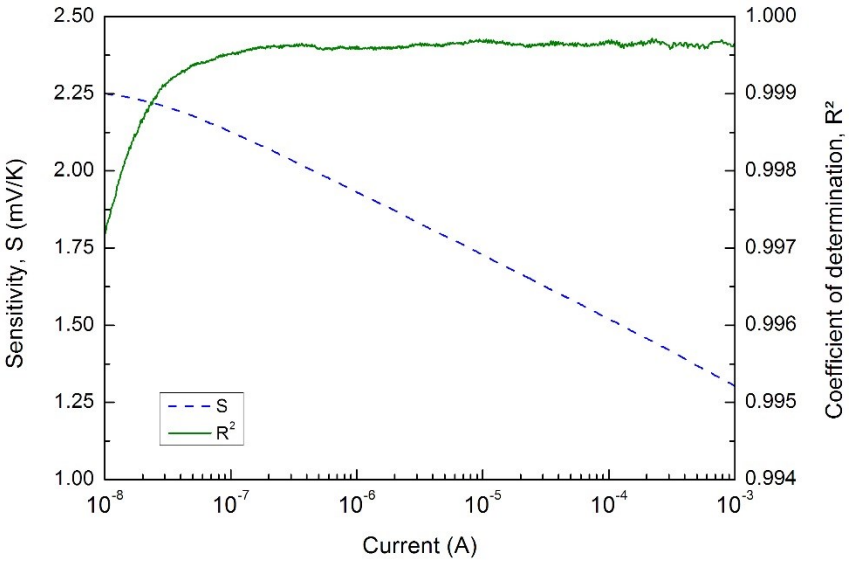
2.50
2.25
2.00
1.75
1.50
1.25
1.00
Sensitivity, S (mV/K)
1.000
0.999
0.998
0.997
0.996
0.995
0.994
Coefficient of determination, R²
S
R²
10⁻⁸
10⁻⁷
10⁻⁶
10⁻⁵
10⁻⁴
10⁻³
Current (A)

Fig. 10

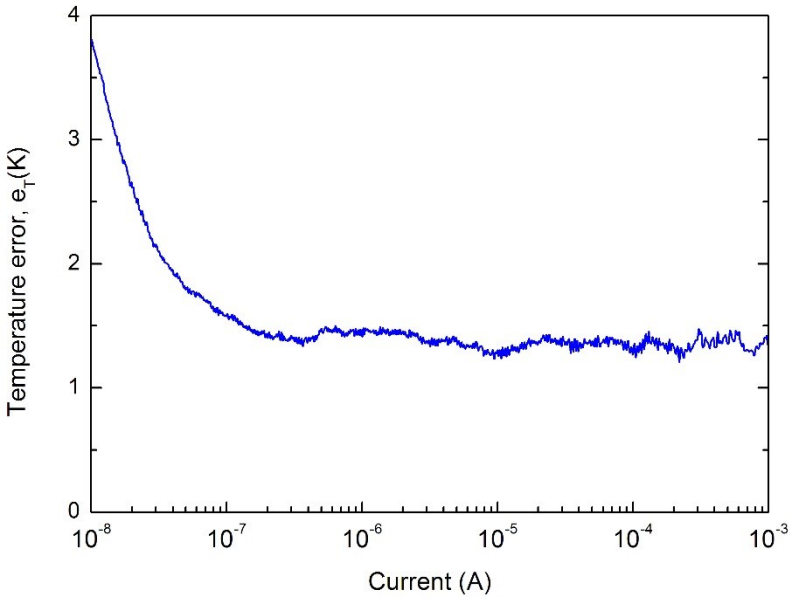
Temperature error, e_T(K)
Current (A)
0
1
2
3
4
10^{-8}
10^{-7}
10^{-6}
10^{-5}
10^{-4}
10^{-3}

Fig. 11

Table I. Apparent band-gap narrowing parameters

	n	*p*
A	1.17×10^{-2}	1.54×10^{-3}
B	1.50×10^{-2}	1.30×10^{-2}
C	1.90×10^{-2}	1.57×10^{-2}

Table II. 4H-SiC carrier mobility parameters

	n	*p*
μ_0^{min}(cm²/Vs)	40	15.9
μ_0^{max}(cm²/Vs)	950	125
N^{crit} (cm^{-3})	2×10^{17}	1.76×10^{19}
α	0.50	0.50
β	2.40	2.15
γ	0.76	0.34
δ	0.76	0.34